Supplementary Material (ESI) for Dalton Transactions
This journal is © The Royal Society of Chemistry

Self-assembly of a molecular crown as a structural analogue of calix[4]arene to modify Keggin anions

Aixiang Tian, Xiaoling Lin, Jun Ying, Juwen Zhang, Hongyan Lin, Guocheng Liu, Dan Zhao, Na Li, Xiuli Wang*

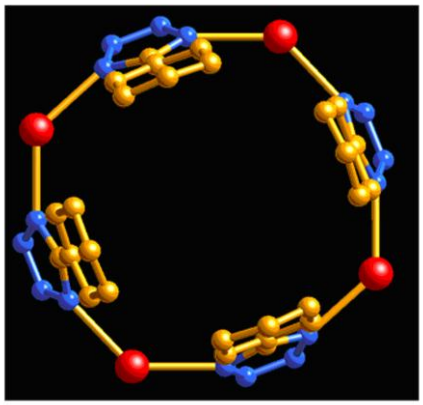

Fig. S1. The $[Ag_4(ptz)_4]$ subunit viewing along the *c* axis showing a four-membered cycle.

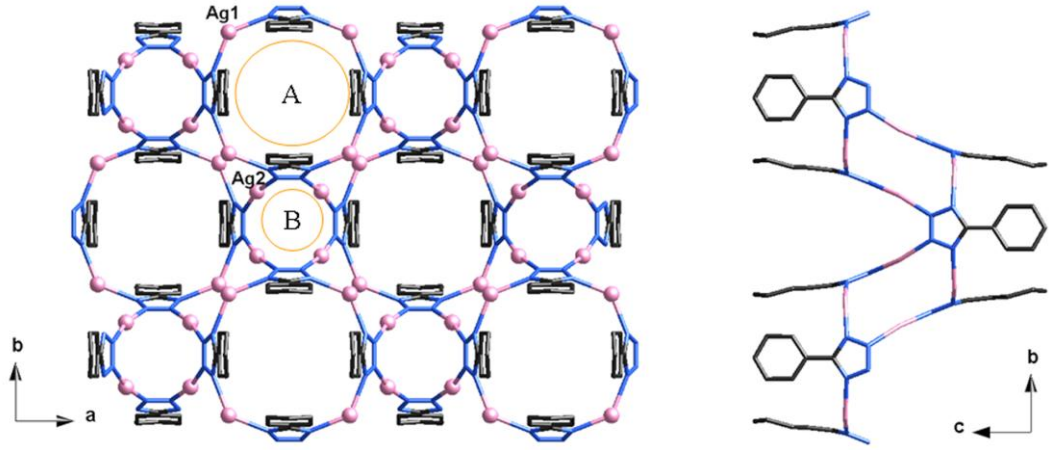

Fig. S2. The 2D metal-organic layer in compound **1** containing two kinds of four-membered cycles A and B, viewing along the *c* (left) and *a* axises (right).

Supplementary Material (ESI) for Dalton Transactions
This journal is © The Royal Society of Chemistry

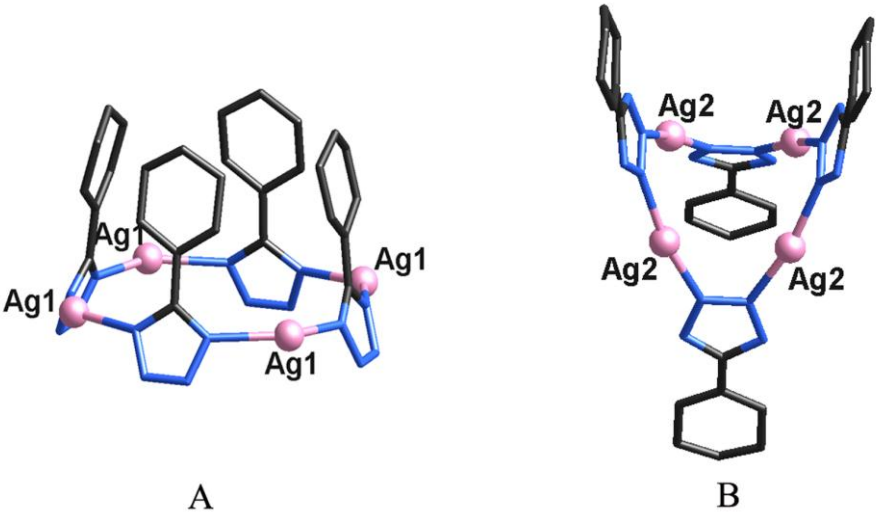

Fig. S3. The bigger four-membered cycle A and smaller one B in the 2D layer.

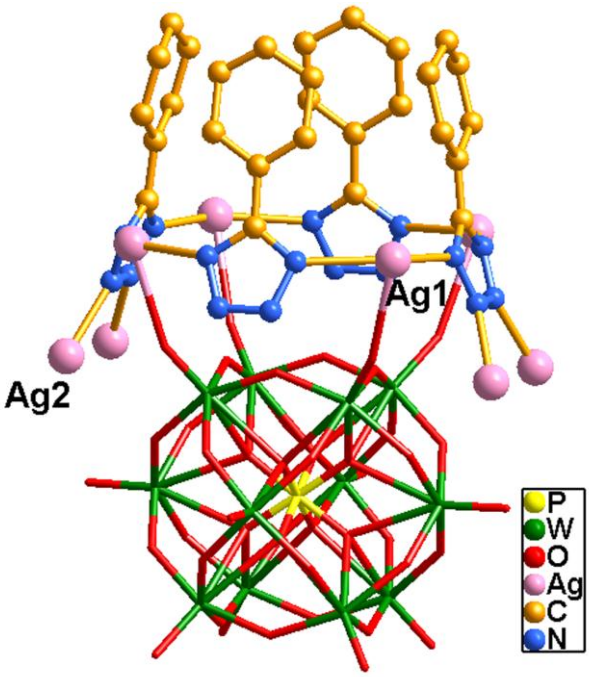

Fig. S4. One anion supports one molecular crown $[Ag_4(ptz)_4]$ through offering four O9 atoms all at the same polar position.

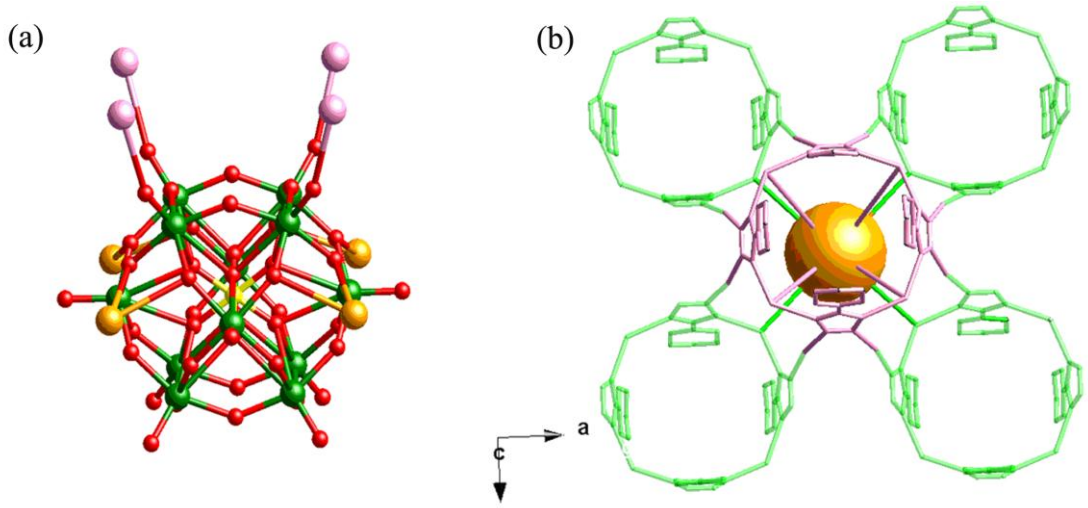

Fig. S5. (a) The PW_{12} anion offers four terminal O9 atoms all at the same "polar" position and eight bridging O7 atoms at the same "belt" position to connect total eight Ag1 ions. (b) The four "polar" Ag ions are from one molecular crown (pink) and four "belt" Ag ions are from four different crowns (green).

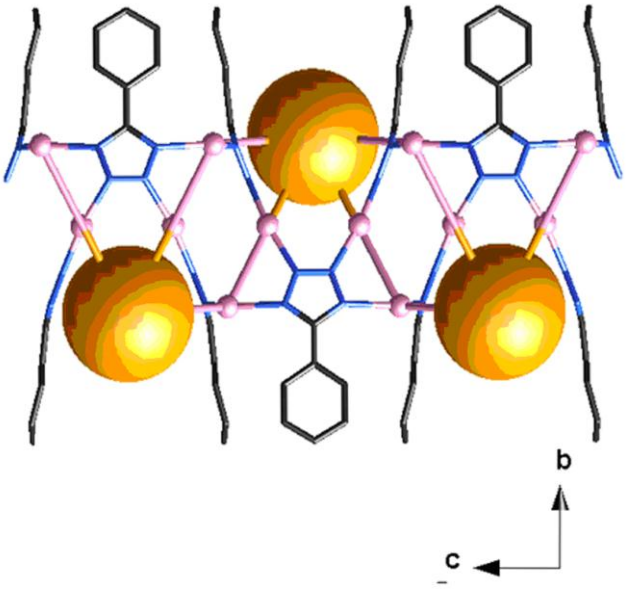

Fig. S6. The anions suspend the 2D metal-organic layer in an up-and-down mode.

Supplementary Material (ESI) for Dalton Transactions
This journal is © The Royal Society of Chemistry

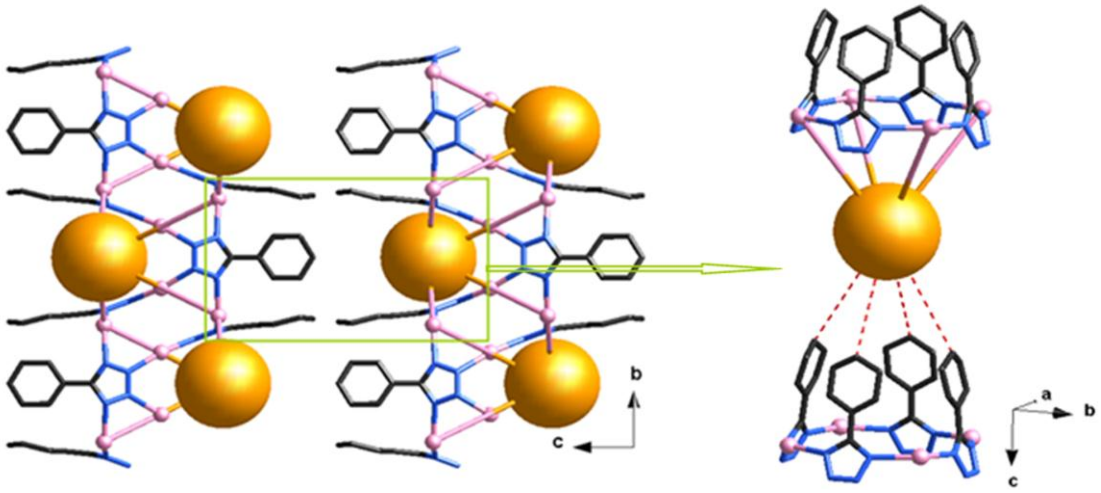

Fig. S7. The abundant hydrogen bonding interactions between the crown and the anion in adjacent layers.

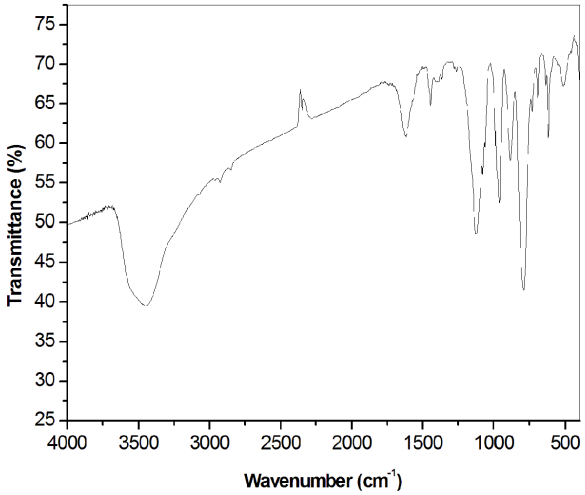

Fig. S8. IR spectrum of compound **1**.

In the spectrum of **1**, characteristic band at 1056 cm^{-1} is attributed to ν(P–O), 962 cm^{-1} is attributed to ν(W–O_d), 885 cm^{-1} is attributed to ν(W–O_b–W), and 794 cm^{-1} is attributed to ν(W–O_c–W). Bands in the regions of 1117–1625 cm^{-1} are characteristic peaks of the ptz ligand.

Supplementary Material (ESI) for Dalton Transactions
This journal is © The Royal Society of Chemistry

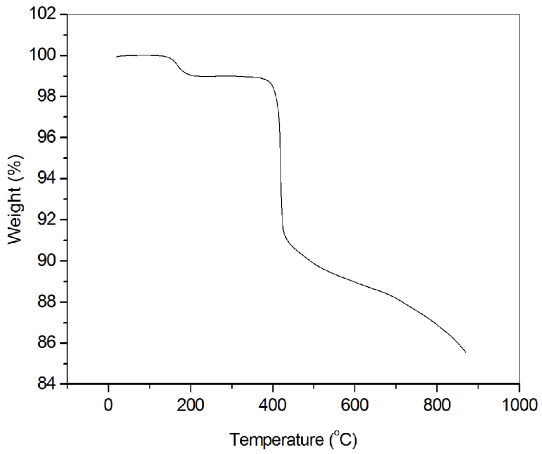

Fig. S9. The TG curve of compound **1**.

The TG experiment was performed under N_2 atmosphere with a heating rate of 10 $^{o}C \cdot min^{-1}$ in the temperature range of 20–850 ^{o}C. The TG curve of compound **1** shows two distinct weight loss steps: The first weight loss step below 250 ^{o}C correspond to the loss of water molecules 0.92% (calcd. 0.83%). The second weight loss step in the range of 300–850 °C can be ascribed to the loss of organic molecules 13.49% (calcd. 14.04%).

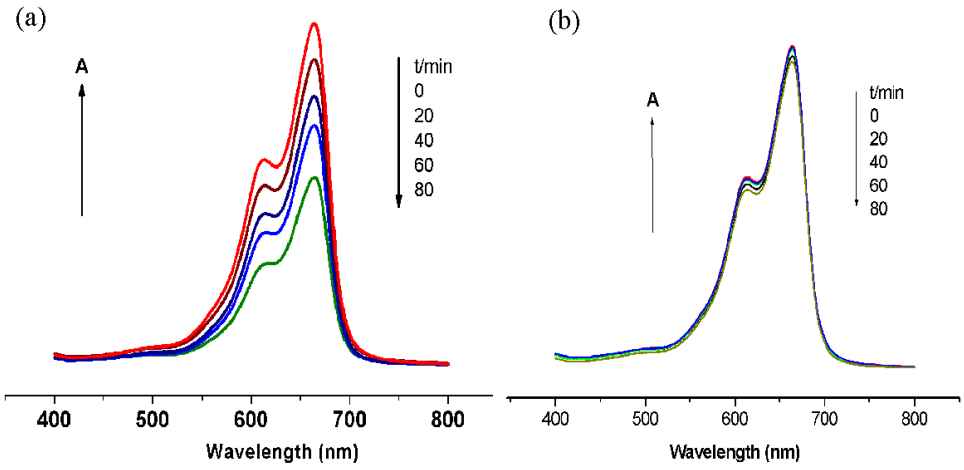

Fig. S10. Absorption spectra of the MB solution during the decomposition reaction under UV light irradiation with the use of compound **1** (a) and without any catalyst (b).

Compound **1** was dispersed in the MB solution (10.0 $mg \cdot L^{-1}$), and the suspension was magnetically stirred in the dark for 30 min to ensure the equilibrium of the working

solution. Then the solution was exposed to UV irradiation from an Hg lamp, kept stirring during irradiations. A sample was taken out every 15 min for analysis.

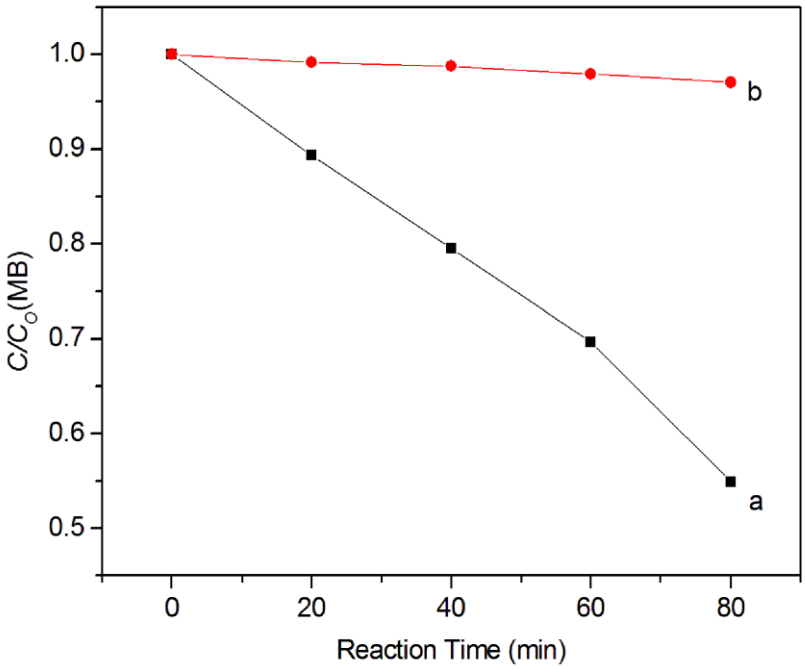

Fig. S11. C/C_0～t curves of MB photocatalytic degradation (a: compound **1**, b: MB only).

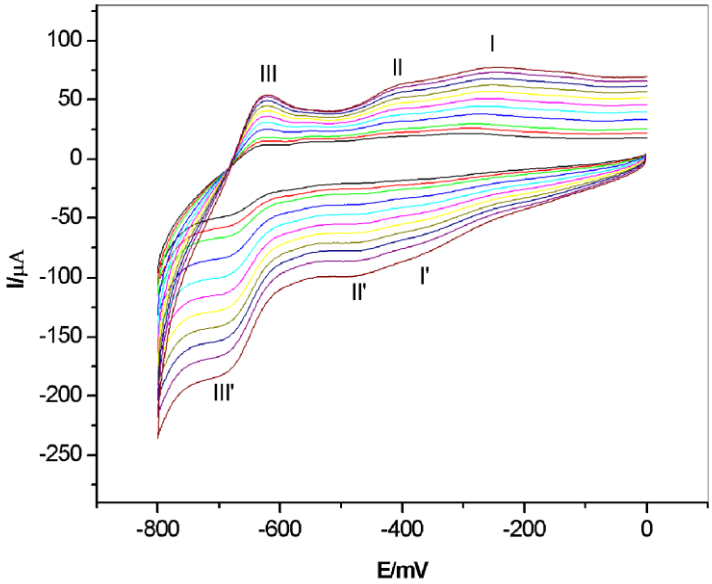

Fig. S12. The cyclic voltammograms of the **1**–CPE in 0.1M H_2SO_4 + 0.5M Na_2SO_4 aqueous solution at different scan rates (from inner to outer: 20, 40, 60, 80, 100, 120, 140, 160, 180, 200 and 220 $mV \cdot s^{-1}$, respectively.).

Supplementary Material (ESI) for Dalton Transactions
This journal is © The Royal Society of Chemistry

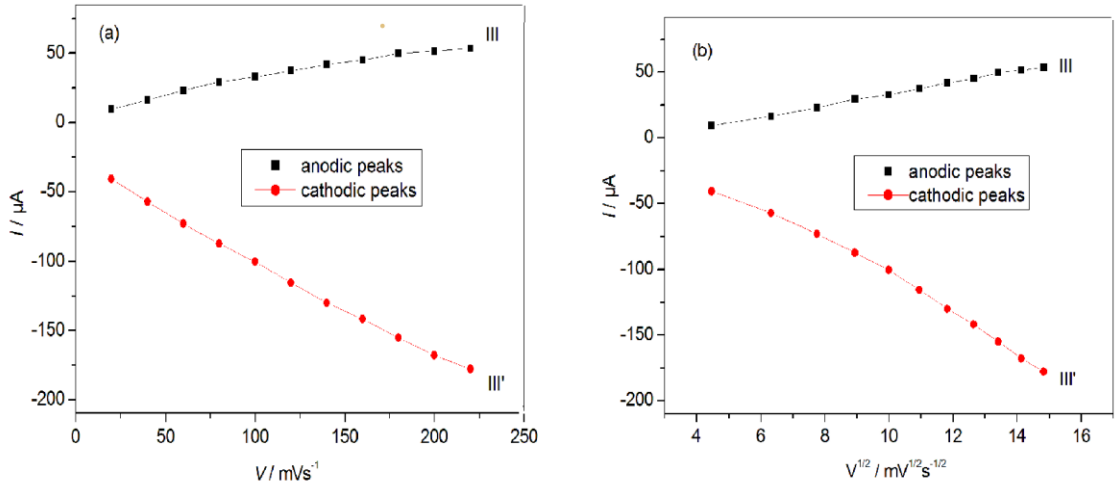

Fig. S13. Plots of the anodic and the cathodic peak III–III′ current against υ (a) and $\upsilon^{1/2}$ (b).

When the scan rates are lower than 80 $mV \cdot s^{-1}$, the peak currents are proportional to the scan rates, which indicates that the redox process of **1**–CPE is surface-confined; however, when the scan rates are higher than 80 $mV \cdot s^{-1}$ the peak currents are proportional to the square root of the scan rates, which indicates that the redox process of **1**–CPE is diffusion-confined.

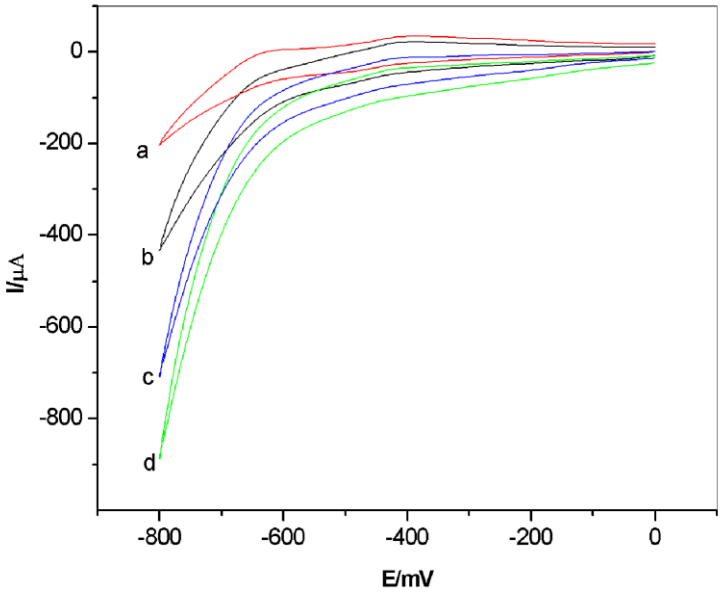

Fig. S14. Cyclic voltammograms of the **1**–CPE in 0.1M H_2SO_4 + 0.5M Na_2SO_4 aqueous solution containing 0(a); 2(b); 4(c) and 6(d) mM $NaNO_2$. Scan rate: 140 $mV \cdot s^{-1}$.

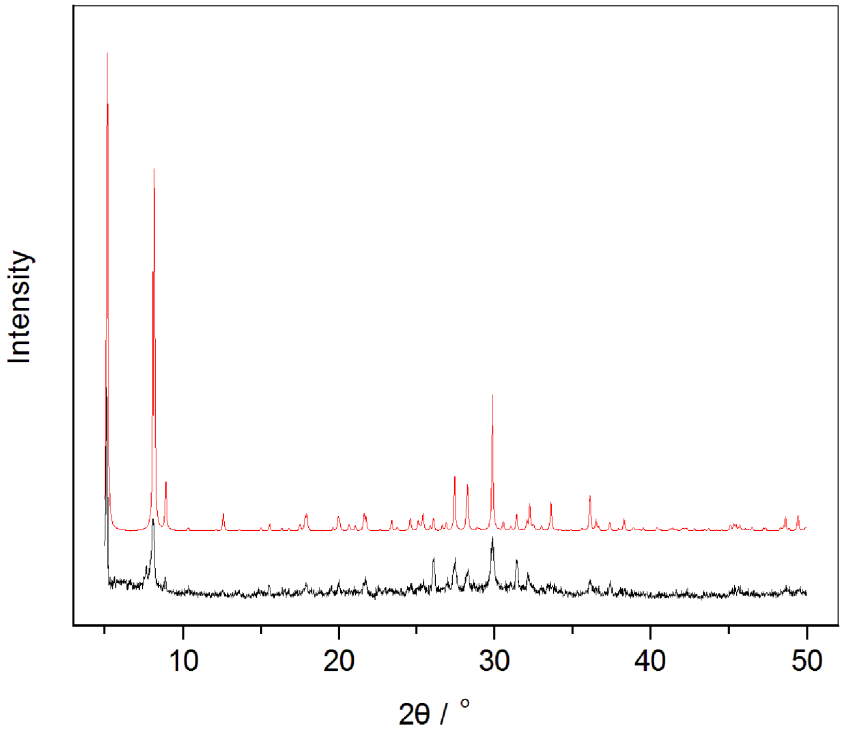

Fig. S15. The simulated (red line) and experimental (black line) powder X-ray diffraction patterns for compound **1**.

Fig. S15 presents the powder X-ray diffraction pattern for compound **1**. The diffraction peaks of both simulated and experimental patterns match well in positions, thus indicating that the phase purity of the compound **1** are well. The difference in reflection intensities between the simulated and experimental patterns is due to the different orientation of the crystals in the powder samples.

Table S1 Crystal data and structure refinement parameters for compound **1**.

formula	$C_{28}H_{24}Ag_8N_{16}O_{42}PW_{12}$
fw	4356.61
cryst syst	Tetragonal
space group	P4/nmm
a (Å)	14.0534(6)
b (Å)	14.0534(6)

Supplementary Material (ESI) for Dalton Transactions
This journal is © The Royal Society of Chemistry

c (Å)	17.0713(14)
V(Å^3)	3371.5(3)
Z	2
D_c (g cm^{-3})	4.288
R_{int}	0.0603
GOF	1.029
R_1[a][I>2sigma(I)]	0.0495
wR_2[b] (all data)	0.1562

[a]$R_1 = \Sigma||F_o|-|F_c||/\Sigma|F_o|$; [b]$wR_2 = \Sigma[w(F_o^2-F_c^2)^2]/\Sigma[w(F_o^2)^2]]^{1/2}$

Table S2 Selected bond lengths (Å) and bond angles (°) for compound **1**.

W(1)-O(9)	1.670(13)	W(1)-O(8)	1.861(7)
W(1)-O(8)#2	1.861(7)	W(1)-O(7)	1.920(10)
W(1)-O(7)#4	1.920(10)	W(1)-O(2)	2.433(13)
W(1)-O(2)#1	2.433(13)	W(2)-O(5)	1.881(10)
W(2)-O(4)	1.642(14)	W(2)-O(5)#5	1.881(10)
W(2)-O(7)	1.892(10)	W(2)-O(7)#5	1.892(10)
W(2)-O(1)#2	2.45(2)	W(2)-O(2)#1	2.480(18)
W(3)-O(6)#1	1.888(8)	W(3)-O(3)	1.658(13)
W(3)-O(5)	1.915(11)	W(3)-O(6)	1.888(8)
W(3)-O(1)#3	2.473(14)	W(3)-O(5)#4	1.915(11)
Ag(1)-N(1)	2.319(10)	W(3)-O(1)#1	2.473(14)
Ag(1)-N(1)#4	2.319(10)	Ag(1)-O(9)	2.655(9)
Ag(2)-N(2)#6	2.163(9)	Ag(1)-O(7)	2.742(10)
N(2)#6-Ag(2)-N(2)	167.2(5)	Ag(2)-N(2)	2.163(9)
N(1)#4-Ag(1)-N(1)	132.6(6)		

Symmetry codes for **1**: #1 -y+1/2,x,z #2 y,-x+1/2,z #3 -x+1/2,-y+1/2,z #4 y,x,z #5 -x+1/2,y,z #6 -y,-x,-z+